On the use of interaction tensors to describe and predict rod interactions in rod suspensions

Julien Férec, Emmanuelle Abisset-Chavanne, Gilles Ausias, Francisco Chinesta

On the use of interaction tensors to describe and predict rod interactions in rod suspensions

Julien Férec · Emmanuelle Abisset-Chavanne · Gilles Ausias · Francisco Chinesta

Abstract Recently, Férec et al. (2009a) proposed a model for nondilute rod-like suspensions, where particle interactions are taking into account via a micromechanical approach. The derived governing equation used the well-known second- and fourth-order orientation tensors ($\mathbf{a_2}$ and $\mathbf{a_4}$) and novel second- and fourth-order interaction tensors ($\mathbf{b_2}$ and $\mathbf{b_4}$). To completely close the model, it is necessary to express $\mathbf{a_4}$, $\mathbf{b_2}$, and $\mathbf{b_4}$ in terms of $\mathbf{a_2}$. This paper gives the general framework to elaborate these new relations. Firstly, approximations for $\mathbf{b_2}$ are developed based on linear combinations of $\mathbf{a_2}$ and $\mathbf{a_4}$. Moreover, a new closure approximation is also derived for $\mathbf{b_4}$, based on the orthotropic fitted closure approach. Unknown parameters are determined by a least-square fitting technique with assumed exact solutions constructed from the probability distribution function (PDF). As numerical solutions for the PDF are difficult to obtain given the nonlinearity of the problem, a combination of steady state solutions is used to generate PDF designed to cover uniformly the entire domain of possible orientations. All these proposed approximations are tested against the particle-based simulations in a variety of flow fields. Improvements of the different approximations are observed, and the couple iORW-CO4P3 gives efficient results.

J. Férec · G. Ausias
Université de Bretagne-Sud, EA 4250, LIMATB, 56100 Lorient, France
e-mail: julien.ferec@univ-ubs.fr

E. Abisset-Chavanne · F. Chinesta
GeM, Ecole Centrale de Nantes, 1 rue de la Noë, 44000 Nantes, France

Keywords Fiber suspension · Closure equations · Constitutive equation · Flow-induced orientation · Orientation tensor · Interaction tensor

Introduction

Nanofibers, carbon nanotubes (CNTs), and nanocrystalline celluloses (NCCs) are now widely investigated in order to modulate polymer functionalities at the nanoscale. As for short fibers at the microscale, these nanoparticles present a rod-like shape and form nanosuspension systems, which exhibit different nanostructures depending on their concentrations. Rod suspensions can be characterized according to their volumetric fraction ϕ of solid particles in the fluid and their aspect ratio $r = L / D$, where L and D are, respectively, their length and diameter. Typically, three distinct regimes are proposed in the literature (Doi and Edwards 1978): dilute, in which $\phi < 1 / r^2$; semi-dilute, $1 / r^2 < \phi < 1 / r$; and concentrated, $\phi > 1 / r$. These three regimes of suspension are represented in Figure 1. By increasing the number of rods, each rod undergoes more and more contacts with its neighbors. Doi and Edwards (1978) and then Ranganathan and Advani (1991) approximated the average number of rods whose centerlines intersect a test tube circumscribing a test rod. Later, Toll (1993) obtained an exact solution for an arbitrary test volume and arbitrary rod length distribution, given the orientation distribution and concentration of the rods. In the particular case of 3-D random orientation and for rods with large aspect ratio, the average number of contact points is given by $N_C = \phi(2r + 6)$ (Toll 1993). Figure 1 also shows that rod interactions are not negligible and play an important role even in the dilute domain. The limit between semi-dilute and concentrated regimes is

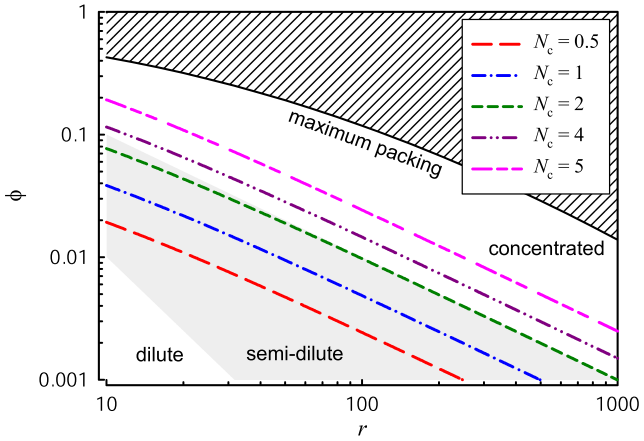

Fig. 1 Rod concentration regimes and average number of contacts per rod, N_C, defined by their volume fraction ϕ and aspect ratio r. The *black line* represents the upper limit of the maximum packing Mueller et al. (2011)

nearly defined by a value of 2 for N_C. The average number of contact per rod is typically larger than 2 in concentrated regime. Solid particles cannot be added to the fluid up to $\phi = 1$. For nonspherical particles, Mueller et al. (2011) proposed to model the maximum packing ϕ_m according to $\phi_m = \phi_m^s \exp\left[-\left(\log_{10} r\right)^2 / 2.3328\right]$, where the maximum packing fraction for spheres, ϕ_m^s, equals 0.656 and is obtained by fitting their data. This upper limit is reported in Fig. 1 with the maximum packing curve.

At the microscale, direct numerical simulations (DNSs) are techniques that can be used to track a rod population, which moves with the suspending fluid and orient depending on the velocity gradient according to the Jeffery equation (Jeffery 1922). Rod interactions have been investigated by DNS (Yamamoto and Matsuoka 1996; Ausias et al. 2006; Yamanoi and Maia 2010a, b). Although of considerable interest to understand the well-defined physics at the microscale level, DNS cannot be easily introduced into commercial software packages owing to their large computational time.

Kinetic theories could also be used to describe such systems at the mesoscopic scale (Doi and Edwards 1986; Bird et al. 1987; Larson 1988). Their main advantage is their capability to address macroscopic systems, while keeping the fine physics through a number of conformational coordinates introduced for describing the microstructure and its time evolution (Keunings 2004; Férec et al. 2008; Férec et al. 2009b; Ma et al. 2008; Ma et al. 2009; Lozinski et al. 2011). At this mesoscopic scale, the microstructure is defined from a probability distribution function (PDF) that depends on the physical space, the time, and a number of conformational coordinates. Their drawback is the large computational time required to solve the PDF equation, although new numerical strategies such as proper generalized decomposition (PGD) are developed (Ammar et al. 2006, 2007). Moments of the PDF are statistical tools that compactly and efficiently describe the microstructure properties. These coarser descriptions are widely used in macroscopic modeling. In order to deal with the orientation description of a rod population, Advani and Tucker (1987) introduced the second- and fourth-order orientation tensors $\mathbf{a_2}$ and $\mathbf{a_4}$. However, the equations governing the time evolution of these conformational moments involve closure approximations, whose impact on the final properties is not yet controlled (Sepehr et al. 2004).

Micromechanical model with rod interactions

The orientation of a particular rod can be described in spherical coordinates by a unit vector $\mathbf{p}^\alpha$ oriented along its axis of revolution. Jeffery (1922) developed an expression for the time evolution of $\mathbf{p}^\alpha$ for a single spheroid suspended in a Newtonian fluid in the absence of external torque. Jeffery equation predicts that the particle aligns in the flow direction and rotates periodically according to the shape factor $\lambda_{\mathbf{p}^\alpha} = \left(r^2 - 1\right)/\left(r^2 + 1\right)$. Later, Folgar and Tucker (1984) improved the Jeffery equation by introducing a diffusion term in order to take into account fiber interactions. This phenomenological term is proportional to the effective deformation rate $|\dot{\gamma}|$ and to a constant diffusion coefficient C_I. This useful model fails to produce slow orientation kinetics for rod suspensions as encountered in nondilute systems due to the interactions (Sepehr et al. 2004). Therefore, Wang et al. (2008) developed the reduced strain closure (RSC) model to capture the slow orientation kinetics. An additional empirical flux is added to the Jeffery motion to modify the growth rates of the eigenvalues of the orientation tensor but to leave the rotation rate expressions for the eigenvectors unchanged. Based on a physical approach at the microscale, Férec et al. (2009a) derived an interaction flux created by the rod-rod interactions, which is added to the Jeffery equation. This interaction flux is obtained from a global torque produced by neighboring rods, which act on the test fiber kinetics. At higher concentration, microstructures involve clusters or aggregates, which can interact to create larger clusters or break due to the hydrodynamic forces (Abisset-Chavanne et al. 2013; Chinesta 2013). To summarize, recent models have been developed to improve the kinematic description of the rod suspensions. In parallel, a lot of works is also devoted to derive anisotropic diffusions. This part will not be reported further in this paper [see Koch (1995), Fan et al. (1998), Jack (2006), and Phelps and Tucker (2009) for more details].

Table 1 Expressions of the pseudo-shape factor $\lambda_{\mathbf{p}^\alpha}$ and the orientation diffusion coefficient D_r for different models taken in the literature

Authors	$\lambda_{\mathbf{p}^\alpha}$	D_r
Jeffery (1922)	$\frac{r^2-1}{r^2+1}$	0
Folgar and Tucker (1984)	1	$C_\mathrm{I}\lvert\dot{\gamma}\rvert$
Advani and Tucker (1987)	$\frac{r^2-1}{r^2+1}$	$C_\mathrm{I}\lvert\dot{\gamma}\rvert$
Férec et al. (2009a)	$1-\phi N_\mathrm{I}\int_{\mathbf{p}^\beta}\lvert\mathbf{p}^\alpha\times\mathbf{p}^\beta\rvert\,\psi_{\mathbf{p}^\beta}d\mathbf{p}^\beta$	$\phi N_\mathrm{I} q\lvert\dot{\gamma}\rvert\int_{\mathbf{p}^\beta}\lvert\mathbf{p}^\alpha\times\mathbf{p}^\beta\rvert\,\psi_{\mathbf{p}^\beta}d\mathbf{p}^\beta$

General orientation dynamic

A fairly general form of the time evolution for rods can be written as:

$$\dot{\mathbf{p}}^\alpha=-\frac{1}{2}\boldsymbol{\omega}\cdot\mathbf{p}^\alpha+\frac{1}{2}\lambda_{\mathbf{p}^\alpha}\left(\dot{\boldsymbol{\gamma}}\cdot\mathbf{p}^\alpha-\dot{\boldsymbol{\gamma}}:\mathbf{p}^\alpha\mathbf{p}^\alpha\mathbf{p}^\alpha\right)-D_\mathrm{r}\frac{\partial\ln\psi_{\mathbf{p}^\alpha}}{\partial\mathbf{p}^\alpha} \tag{1}$$

where $\boldsymbol{\omega}$ and $\dot{\boldsymbol{\gamma}}$ are the vorticity and deformation rate tensors, respectively. D_r is a rotary diffusivity that introduces an isotropic diffusion. $\psi_{\mathbf{p}^\alpha}$ represents the probability to find a rod with an orientation of $\mathbf{p}^\alpha$, and $\lambda_{\mathbf{p}^\alpha}$ is a pseudo-shape factor. Table 1 gives the expressions of D_r and $\lambda_{\mathbf{p}^\alpha}$ for some previous described models.

In what follows, the focus is carried out on the model proposed by Férec et al. (2009a), as we would like to highlight the effects induced by the rod interactions on the convective part; therefore, D_r is fixed to zero. In this model, $\lambda_{\mathbf{p}^\alpha}$ is a pseudo-shape factor that is a function of $\mathbf{p}^\alpha$ and is given by:

$$\lambda_{\mathbf{p}^\alpha}=1-\phi N_\mathrm{I}\int_{\mathbf{p}^\beta}\left|\mathbf{p}^\alpha\times\mathbf{p}^\beta\right|\psi_{\mathbf{p}^\beta}d\mathbf{p}^\beta, \tag{2}$$

where N_I is a dimensionless scalar that relates the intensity of the friction between particles. The test rod is denoted by the superscript α, whereas the superscript β refers to the neighboring rod. The Onsager potential $\left|\mathbf{p}^\alpha\times\mathbf{p}^\beta\right|$ is maximum and equals one when two rods interact orthogonally and is minimum and null when two rods are both parallel Onsager (1949). The average over the orientation space for the neighboring rod enables the model to integrate the effect of interaction into the convective part. Intuitively, it results that the pseudo-shape factor tends to reach the limit value of one when the rods become perfectly aligned. This special case occurs when a test rod is surrounded by neighboring rods that are all aligned parallel to the streamlines. Moreover, it is possible that $\left|\lambda_{\mathbf{p}^\alpha}\right|\geq 1$ depending on the value assigned to ϕN_I. The behavior of an axisymmetric body for which $|\lambda|\geq 1$, ultimately adopts a stable steady state orientation independent of its initial orientation [see Ericksen (1960), Bretherton (1962), and Brenner (1974) for more details]. For nondilute suspensions, it seems possible that interactions between neighboring rods might sometimes act similarly Ericksen (1960). When the low volume fraction is low or the rods are fully aligned, Eq. (1) associated with Eq. (2) leads to the equation of motion for slender particle (Dinh and Armstrong 1984).

Macroscopic time evolution of the microstructure

Using the continuity equation for the probability distribution function and Eqs. (1) and (2), the convective part of the dynamic change for the second-order orientation tensor $\mathbf{a_2}$ is obtained easily without any approximation (diffusion is neglected) and yields to:

$$\begin{aligned}\frac{D\mathbf{a_2}}{Dt}&=-\frac{1}{2}\left(\boldsymbol{\omega}\cdot\mathbf{a_2}-\mathbf{a_2}\cdot\boldsymbol{\omega}\right)+\frac{1}{2}\left(\dot{\boldsymbol{\gamma}}\cdot\mathbf{a_2}+\mathbf{a_2}\cdot\dot{\boldsymbol{\gamma}}-2\dot{\boldsymbol{\gamma}}:\boldsymbol{a_4}\right)\\&\quad-\frac{1}{2}\phi N_\mathrm{I}\left(\dot{\boldsymbol{\gamma}}\cdot\mathbf{b_2}+\mathbf{b_2}\cdot\dot{\boldsymbol{\gamma}}-2\dot{\boldsymbol{\gamma}}:\boldsymbol{b_4}\right).\end{aligned} \tag{3}$$

$\mathbf{a_2}$ and $\mathbf{a_4}$ are the second- and fourth-order orientation tensors defined as (Advani and Tucker 1987):

$$\mathbf{a_2}=\int_{\mathbf{p}^\alpha}\mathbf{p}^\alpha\mathbf{p}^\alpha\psi_{\mathbf{p}^\alpha}d\mathbf{p}^\alpha, \tag{4}$$

$$\mathbf{a_4}=\int_{\mathbf{p}^\alpha}\mathbf{p}^\alpha\mathbf{p}^\alpha\mathbf{p}^\alpha\mathbf{p}^\alpha\psi_{\mathbf{p}^\alpha}d\mathbf{p}^\alpha. \tag{5}$$

The second- and fourth-order interaction tensors $\mathbf{b_2}$ and $\mathbf{b_4}$ are given by (Férec et al. 2009a):

$$\mathbf{b_2}=\int_{\mathbf{p}^\alpha}\int_{\mathbf{p}^\beta}\mathbf{p}^\alpha\mathbf{p}^\alpha\left|\mathbf{p}^\alpha\times\mathbf{p}^\beta\right|\psi_{\mathbf{p}^\alpha}\psi_{\mathbf{p}^\beta}d\mathbf{p}^\beta d\mathbf{p}^\alpha, \tag{6}$$

$$\mathbf{b_4}=\int_{\mathbf{p}^\alpha}\int_{\mathbf{p}^\beta}\mathbf{p}^\alpha\mathbf{p}^\alpha\mathbf{p}^\alpha\mathbf{p}^\alpha\left|\mathbf{p}^\alpha\times\mathbf{p}^\beta\right|\psi_{\mathbf{p}^\alpha}\psi_{\mathbf{p}^\beta}d\mathbf{p}^\beta d\mathbf{p}^\alpha. \tag{7}$$

Interaction tensors are completely symmetric and are defined by forming the dyadic products of the vector $\mathbf{p}^\alpha$, weighted by the Onsager potential $\left|\mathbf{p}^\alpha\times\mathbf{p}^\beta\right|$, and then twice integrating the product with respect to the distribution function over all possible directions. The trace of the second-order interaction $\mathbf{b_2}$ is directly proportional to the average number of contacts per rods N_C (Férec et al. 2009a). It is known that orientation tensors give a statistical average for the orientation of a rod population (Advani and Tucker 1987). It means that the $\mathbf{a_2}$ components are indistinguishable between a planar random and biaxial orientation state, while

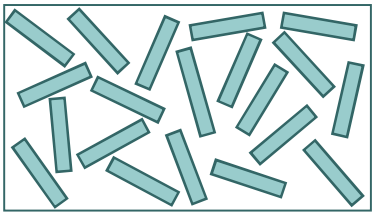

$$\mathbf{a_2} = \begin{bmatrix} 1/2 & 0 & 0 \\ 0 & 1/2 & 0 \\ 0 & 0 & 0 \end{bmatrix} \quad \mathbf{b_2} = \begin{bmatrix} 1/\pi & 0 & 0 \\ 0 & 1/\pi & 0 \\ 0 & 0 & 0 \end{bmatrix}$$

(a)

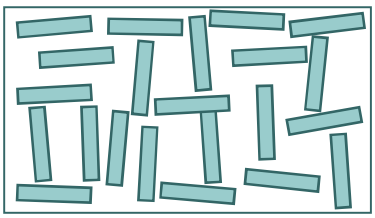

$$\mathbf{a_2} = \begin{bmatrix} 1/2 & 0 & 0 \\ 0 & 1/2 & 0 \\ 0 & 0 & 0 \end{bmatrix} \quad \mathbf{b_2} = \begin{bmatrix} 1/4 & 0 & 0 \\ 0 & 1/4 & 0 \\ 0 & 0 & 0 \end{bmatrix}$$

(b)

Fig. 2 Examples of different orientation states: **a** Planar random in the 1–2 plane. **b** Biaxial orientation

interaction tensors, $\mathbf{b_2}$, differentiate these two orientation states (Fig. 2). Table 2 gives some component values of $\mathbf{a_2}$ and $\mathbf{b_2}$ for simple orientation states (i.e., random isotropic orientation, triaxial orientation. . .).

In summary, Eq. (3) gives the time evolution for $\mathbf{a_2}$. Open questions are as follows: Is it necessary to derive the time evolution for $\mathbf{a_4}$, $\mathbf{b_2}$, and $\mathbf{b_4}$? Or better, is it possible to express $\mathbf{a_4}$, $\mathbf{b_2}$, and $\mathbf{b_4}$ as a function of $\mathbf{a_2}$? Therefore, in this paper, we aimed at developing an orthotropic fitted closure approximation for the fourth-order interaction tensor and a simple way to express the second-order interaction tensor as functions of the orientation tensors. First, particle-based simulations are used to investigate the effect of rod-rod interaction on the convective part in the time evolution of the second-order orientation tensor. The obtained results are also used to test the accuracy of the proposed approximations. Next, we presented the theory behind the orthotropic closure approximation extended for interaction tensors. We also justify how to determine the second-order interaction tensor with a quadratic form in terms of $\mathbf{a_2}$ and a linear combination in terms of $\mathbf{a_2}$ and $\mathbf{a_4}$. As the associated Fokker-Planck equation is numerically difficult to solve, a new strategy is used based on the steady state solutions for the PDF, where different combinations of flow fields are employed and interactions are neglected. Then, unknown parameters for the different approximations are determined using a least-square fitting technique. Finally, we test the new approximations by comparing them to solutions based on particle-based simulations in a basic simple shear flow. Then, numerical calculations are performed to examine their predictability for benchmark problems: tests included a homogeneous simple shear flow and a shear/stretch combined flow and an unsteady combined flow (an isothermal Newtonian radial diverging flow). The proposed approximations represent a substantial improvement over the previous forms in terms of predicting flow-induced rod orientation.

Particle-based simulations

Particle-based simulations are used to investigate the behavior prediction from Eqs. (1) and (2) with $D_\mathrm{r} = 0$, as we would like to highlight the effects of interactions on the convection (Chinesta et al. 2003; Chiba et al. 2005; Chiba and Chinesta 2005). It results to solve Eq. (3) if the particle number is sufficiently large. Thus, rods with different initial orientations are introduced into a material point, and the orientation evolution of each rod is computed. Second-order tensors such as $\mathbf{a_2}$ and $\mathbf{b_2}$ are then evaluated with the following discrete summations:

$$a_{ij} = \frac{1}{N_\mathrm{rod}} \sum_\alpha p_i^\alpha p_j^\alpha, \tag{8}$$

$$b_{ij} = \frac{1}{N_\mathrm{rod}^2} \sum_\alpha \sum_\beta \left| \mathbf{p}^\alpha \times \mathbf{p}^\beta \right| p_i^\alpha p_j^\alpha. \tag{9}$$

Table 2 Examples of $\mathbf{a_2}$ and $\mathbf{b_2}$ components for particular rod orientation states

Orientation state	a_{11}	a_{22}	a_{33}	b_{11}	b_{22}	b_{33}
Unidirectional (aligned in 1-direction)	1	0	0	0	0	0
2-D random in the 1–2 plane	1/2	1/2	0	$1/\pi$	$1/\pi$	0
2-D biaxial orientation (1- and 2-directions)	1/2	1/2	0	1/4	1/4	0
3-D random	1/3	1/3	1/3	$\pi/12$	$\pi/12$	$\pi/12$
3-D triaxial orientation	1/3	1/3	1/3	2/9	2/9	2/9

Using $N_{\text{rod}} = 1000$ particles is not enough to guarantee accurate solutions, whereas $N_{\text{rod}} = 50000$ particles give significant results with high computational time. Therefore, 10000 particles are found to be a relative good compromise between accuracy and computational time. An explicit scheme is used to integrate Eqs. (1) and (2) with a time step of $\Delta t = 0.05$ s and an applied shear rate of 1 s^{-1}. No numerical diffusion was observed in the sense that in the reverse simple shear flow (i.e., a negative constant shear rate is applied), the initial solutions are recovered. This also suggests that Eq. (1) associated with Eq. (2) is purely convective, and interaction terms do not introduce any diffusion. Figure 3a presents the time evolutions of a_{11} and a_{12} in simple shear flow as functions of time and for different values of the ϕN_{I} number, with an initial isotropic rod orientation. The applied shear rate is $\dot{\gamma} = 1$ s^{-1}. For $\phi N_{\text{I}} = 0$, the Jeffery solution is obtained with an infinite aspect ratio, therefore inducing that $\lambda_{\mathbf{p}^\alpha} = 1$. By increasing ϕN_{I}, the time evolutions of a_{11} and a_{12} evolved differently: interactions perturb the convection. A transient regime is observed until 60 s, and then, the rod population rotates periodically with the same amplitude. In the case where the shape parameter is constant and less than 1 (i.e., $\lambda_{\mathbf{p}^\alpha} = 0.9$), a_{11} and a_{12} oscillate at a well-known period of $T = 2\pi\left(r + r^{-1}\right)/\dot{\gamma}$ (Petrie 1999) with a constant amplitude, and no transients are observed. It results that the interaction model induces a strong modification in the rod kinematics. Figure 3b shows the time evolutions of a_{11} and a_{22} in uniaxial elongational flow as functions of time and for different values of the ϕN_{I} number, with an initial isotropic rod orientation. The Hencky strain rate is 1 s^{-1}. Slow orientation kinetics in rod suspensions are observed by increasing ϕN_{I}, indicating that the steady state regime is delayed by the interaction model.

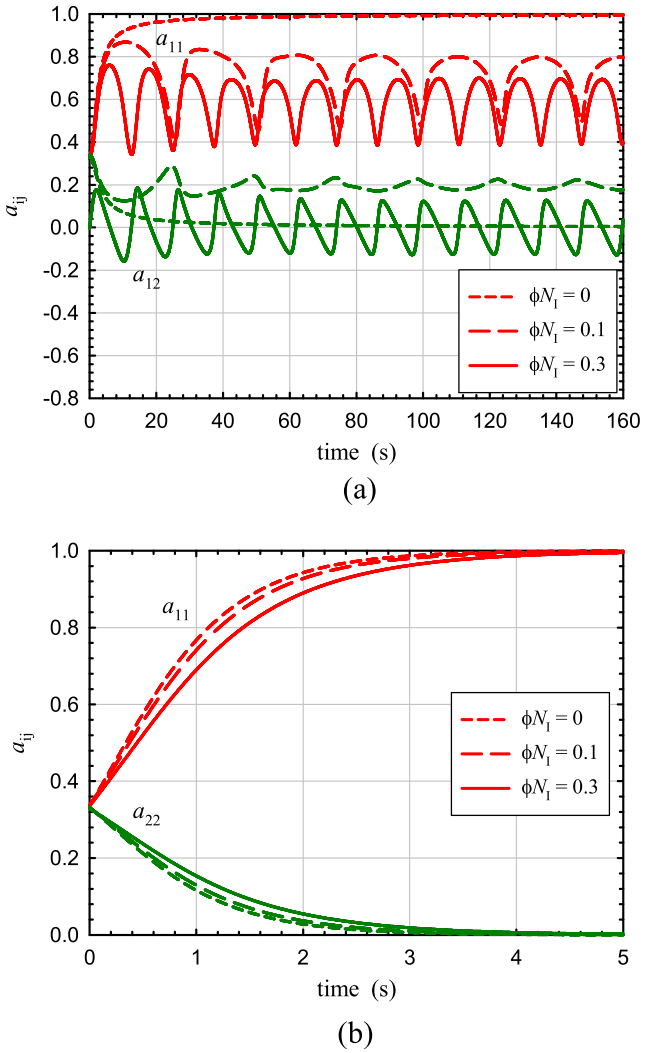

Fig. 3 Variations of the $\mathbf{a_2}$ components as function of time for different values of ϕN_{I}. **a** a_{11} and a_{12} tensor components for simple shear flow at a shear rate of 1 s^{-1}. **b** a_{11} and a_{12} tensor components of a_2 for uniaxial elongational flow at a Hencky rate of 1 s^{-1}

Approximation developments

Equation (3) gives the time evolution of the microstructure at the macroscopic scale. In order to achieve to a complete set of rheological equations, some relations are needed to specify the fourth-order orientation tensor $\mathbf{a_4}$ and both interaction tensors $\mathbf{b_2}$ and $\mathbf{b_4}$. The first approximation is a closure that relates $\mathbf{a_4}$ to $\mathbf{a_2}$. Many works have been proposed in the literature but will not be reported further in this paper [see Chung and Kwon (2001), Sepehr et al. (2004), Kröger et al. (2008), Pruliere et al. (2009), and Jack et al. (2010) for more details]. The ORW3 closure approximation (orthotropic fitted closure approximation for wide C_{I} values with third-order polynomial expansions) developed by Chung and Kwon (2001) is chosen to evaluate the fourth-order orientation tensor. Similarly, a second closure approximation is required to determine $\mathbf{b_4}$ as a function of $\mathbf{b_2}$. The following section deals with this problem. Finally, it remains to find a way to express the second-order interaction tensor $\mathbf{b_2}$.

Approximations for the second-order interaction tensor

Up to now, two strategies are available to evaluate the second-order interaction tensor $\mathbf{b_2}$. The first one consists in deriving the time evolution equation for $\mathbf{b_2}$. Besides the difficulties to obtain this equation, some closure approximations will be necessary, and this procedure will not be developed in what follows. The second possibility is to express $\mathbf{b_2}$ directly from the orientation tensors. This approach is physically justified: from their definitions, orientation, and interaction tensors [Eqs. (4)–(7)] are functions of the probability distribution function. Furthermore, Advani and Tucker (1987) showed that the probability

distribution function can be recovered in terms of orientation tensors, that is $\psi_{\mathbf{p}^\alpha} = \psi_{\mathbf{p}^\alpha}(\boldsymbol{\delta}, \mathbf{a_2}, \mathbf{a_4}, \mathbf{a_6}, \ldots)$ where $\boldsymbol{\delta}$ is the identity tensor. Therefore, the second-order interaction tensor can be written as a function of orientation tensors such as $\mathbf{b_2} = \mathbf{b_2}(\boldsymbol{\delta}, \mathbf{a_2}, \mathbf{a_4}, \mathbf{a_6}, \ldots)$. Generally, closure approximations for the orientation tensors mention that the $(2n+2)$th-order orientation tensor is constructed from the $(2p)$th-order orientation tensors with $p \leq n$. Furthermore, the Cayley-Hamilton theorem states that $\mathbf{a_2}$ satisfies its own characteristic equation. In 3-D, it means that any powers of $\mathbf{a_2}$ higher than 3 can be calculated using $\boldsymbol{\delta}$, $\mathbf{a_2}$, and $\mathbf{a_2^2}$. Therefore, we proposed the two following approximations for $\mathbf{b_2}$:

$$\mathbf{b_2} = \beta_1\boldsymbol{\delta} + \beta_2\mathbf{a_2} + \beta_3\mathbf{a_2^2}, \tag{10}$$

and

$$\mathbf{b_2} = \beta_1\boldsymbol{\delta} + \beta_2\mathbf{a_2} + \beta_3\mathbf{a_4}\colon\delta + \beta_4\mathbf{a_4}\colon\mathbf{a_2}. \tag{11}$$

The first expression [Eq. (10)] is a quadratic form in terms of $\mathbf{a_2}$, and Eq. (11) is a linear combination in terms of $\mathbf{a_2}$ and $\mathbf{a_4}$. We note that the initial relation given by Férec et al. (2009a) is:

$$\mathbf{b_2} = \frac{3\pi}{8}(\mathbf{a_2} - \mathbf{a_4}\colon\mathbf{a_2}). \tag{12}$$

Equation (12) is recovered from Eq. (11) if $\beta_1 = \beta_3 = 0$ and $\beta_2 = -\beta_4 = 3\pi/8$. Both relations (10) and (11) assume that the $\beta_1, ..., \beta_3$ and $\beta_1, ..., \beta_6$ coefficients are functions of the second and third invariant of $\mathbf{a_2}$, $I_2 = \text{trace}\ \mathbf{a_2}\cdot\mathbf{a_2}$ and $I_3 = \text{trace}\ \mathbf{a_2}\cdot\mathbf{a_2}\cdot\mathbf{a_2}$. There is no specific principle for choosing the functional expressions, so in the present work, the $\beta_1, ..., \beta_3$ and $\beta_1, ..., \beta_6$ coefficients are taken to be polynomial functions of I_2 and I_3 such as:

$$\beta_m = a_m^1 + a_m^2 I_2 + a_m^3 I_3 + a_m^4 I_2^2 + a_m^5 I_3^2 + a_m^6 I_2 I_3, \tag{13}$$

and

$$\begin{aligned}\beta_m = {} & a_m^1 + a_m^2 I_2 + a_m^3 I_3 + a_m^4 I_2^2 + a_m^5 I_3^2 + a_m^6 I_2 I_3 \\ & + a_m^7 I_2^3 + a_m^8 I_3^3 + a_m^9 I_2^2 I_3 + a_m^{10} I_2 I_3^2,\end{aligned} \tag{14}$$

where the parameters a_m^k are obtained by a fitting procedure described in the PDF generation section.

Closure approximation for the fourth-order interaction tensor

Férec et al. (2009a) proposed two simple closures: one formulated with a linear combination iLIN and the second one based on the quadratic formulation iQUA. They mentioned that the iQUA closure is more relevant than the iLIN closure and its definition is:

$$\mathbf{b_4} = \mathbf{b_2}\mathbf{b_2}/\text{trace}\ \mathbf{b_2}. \tag{15}$$

No other closure approximations are available in the literature. Hence, we propose to improve the interaction closure based on an orthotropic fitted closure. This approach uses the eigenvalues of $\mathbf{b_2}$ in the eigenspace system defined by the eigenvectors of $\mathbf{b_2}$ to derive functional expressions that best fit some flow data. In the framework of orthotropic closure approximations, the principal directions of the fourth-order orthotropic interaction tensor are the same as the eigenvectors of $\mathbf{b_2}$ in order to be objective in tensor representation. As $\mathbf{b_2}$ is a fully symmetric tensor, it has three orthogonal eigenvectors and three corresponding eigenvalues λ_1^i, λ_2^i, and λ_3^i, and its diagonal components must always belong to $[0; \pi/12]$. As compared to $\mathbf{a_2}$, the three eigenvalues of $\mathbf{b_2}$ are required, as its trace is not constant. In addition, these eigenvalues are sorted such as $\lambda_1^i \geq \lambda_2^i \geq \lambda_3^i$. Orthotropic properties (i.e., full symmetry and normalization conditions) imply that only three principal values of $\mathbf{b_4}$ are independent (denoted by $\overline{B}_{11}$, $\overline{B}_{22}$, and $\overline{B}_{33}$) in its principal axis system. To obtain a suitable closure approximation, we introduce specific functional as:

$$\begin{aligned}\overline{B}_{mm}^{\text{closure}} = {} & C_m^1 + C_m^2\lambda_1^i + C_m^3\lambda_2^i + C_m^4\lambda_3^i + C_m^5\left[\lambda_1^i\right]^2 \\ & + C_m^6\left[\lambda_2^i\right]^2 + C_m^7\left[\lambda_3^i\right]^2 + C_m^8\lambda_1^i\lambda_2^i + C_m^9\lambda_1^i\lambda_3^i \\ & + C_m^{10}\lambda_2^i\lambda_3^i.\end{aligned} \tag{16}$$

$m = 1,..., 3$, no sum on m. The fitting of the 30 unknown coefficients C_m^k in Eq. (16) is a process of minimizing the difference between the fitted and some exact components of $\mathbf{b_4}$. This approximation closure is called the iORT closure as reference for orthotropic fitted closure approximation for interaction tensors.

PDF generation

The domain of realistic rod orientation states forms an orientation triangle in the space of the two largest eigenvalues λ_1 and λ_2 of the orientation tensor $\mathbf{a_2}$ (Cintra and Tucker 1995). The three boundary corners of the orientation eigenvalue map consist of a uniaxial orientation (U), where all rods are aligned in a single direction, biaxial orientation states (B) such as random in plane, and triaxial orientation states (T) such as isotropic orientation.

Usually, some flow fields are selected to cover most of the UBT triangle region (Cintra and Tucker 1995; Chung and Kwon 2001; Jack et al. 2010). Then, the associated Fokker-Planck equation is numerically solved and its corresponding moments, such as orientation tensors, are evaluated from the probability distribution function. A lot of care is devoted when different ending times have to be chosen for each flow in order to cover the transient regime and contain the final steady state without overemphasizing the steady state results.

In our case, numerical solutions for the probability distribution function are not yet available as the problem is nonlinear (i.e., the convection part is function of the PDF).

Therefore, we suggest that the probability distribution function is the steady state solution of a flow that combines diffusion, shear, and elongational flows such as:

$$\psi = K_{\text{norm}} \left(C_1 \psi_{\text{shear}} + C_2 \psi_{\text{elongation}} + C_3 \frac{1}{4\pi} \right), \quad (17)$$

where ψ_{shear} and $\psi_{\text{elongation}}$ are the analytical solutions of the distribution function for the Jeffery equation with an infinite aspect ratio and are given by:

$$\psi_{\text{shear,elongation}} = \frac{1}{4\pi} \left[1 + \boldsymbol{\gamma}^{[0]}_{\text{shear,elongation}} : \mathbf{pp} \right]^{-3/2}. \quad (18)$$

$\boldsymbol{\gamma}^{[0]}$ is the finite strain tensor, and its expressions for shear and elongational flows are (Morrison 2001)

$$\boldsymbol{\gamma}^{[0]}_{\text{shear}} = \begin{bmatrix} 0 & -\gamma & 0 \\ -\gamma & \gamma^2 + 1 & 0 \\ 0 & 0 & 0 \end{bmatrix}, \quad (19)$$

$$\boldsymbol{\gamma}^{[0]}_{\text{elongation}} = \begin{bmatrix} e^{\varepsilon(1+b)} - 1 & 0 & 0 \\ 0 & e^{\varepsilon(1-b)} - 1 & 0 \\ 0 & 0 & e^{-2\varepsilon} - 1 \end{bmatrix}. \quad (20)$$

γ and ε are the shear and elongational strains, respectively. The b values state if the elongation is uniaxial, biaxial, or planar (Morrison 2001). In what follows, diffusion is neglected, so C_3 is set to 0.

In order to generate a variety of orientation states that covers uniformly the UBT triangle, its surface is discretized into elementary triangles. Three meshes containing 135, 540, and 2160 elements are tested. An iterative loop is carried out to randomize the γ, ε, b, C_1, and C_2 values to span the UBT region. Convergence is reached when a single probability distribution function is assigned at each elementary triangle. The meshing grid for the surface of the PDF is composed of 70 $\times$ 70 cells to obtain accurate solutions for nearly aligned rod orientation states (Férec et al. 2008). Figure 4 shows the mesh with 135 elements and the points where a PDF is defined. This procedure ensures that the UBT triangle is uniformly covered and removes the difficulties in the selection of the training data set at the ending time.

Once a database of probability distribution functions is obtained, the components for the orientation and interaction tensors are calculated. Then, the C^k_m and a^k_m coefficients are adjusted to minimize the difference between the components predicted by the proposed approximations and those calculated from the PDF. The minimization was carried out using the trust region-reflective algorithm. A constrain is added to the minimization process. For eigenvalues higher than 0.98, a null tensor is imposed to $\mathbf{b_2}$. In this region, the rods are nearly perfectly aligned; therefore, the PDF is closed to a Dirac delta function, and the used mesh is unable to calculate accurate orientation and interaction tensors. The mesh containing 2160 elementary triangles is found to give the best results. The C^k_m coefficients for the interaction

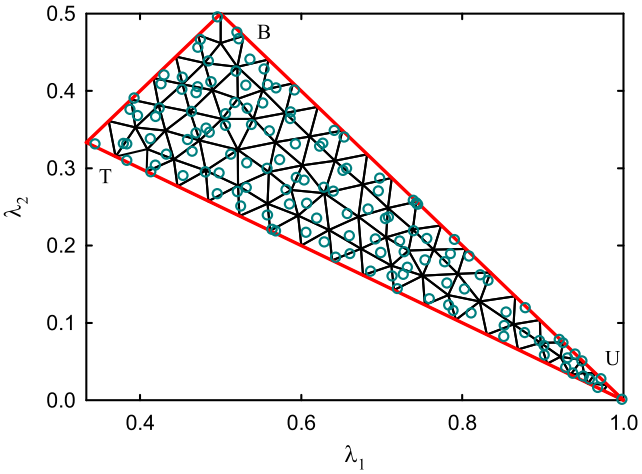

Fig. 4 UBT triangle for the all possible rod orientation states and the used meshing (the grid is composed of 135 elementary triangles). Also shown in circles are points where PDF are defined

closure approximation are given in Appendix 1. In what follows, results with approximation using a quadratic form in terms of $\mathbf{a_2}$ to express $\mathbf{b_2}$ [Eq. (10)] are not shown, as expression (11) reveals to be more accurate. CO4P2 and CO4P3 use a second- and a third-order polynomial function of I_2 and I_3, respectively [Eqs. (13) and (14)]. The values of the independent parameters a^k_m are presented in the Appendices 2 and 3.

Validation of the approximations

Advani and Tucker (1990) revealed the significance of checking approximations in a diversity of flow fields. Different steady state flows that cover a variety of orientation states are used to generate the approximations (i.e., iORT orthotropic fitted closure, CO4P2 and CO4P3 relations). Therefore, some tests are performed in simple shear flows, as these flows were not used to derive the approximations. Therefore, it is possible to check a posteriori how well the low-dimensional approximations compare against the particle-based simulations. The following results are obtained with the couple iORW-CO4P3 for convenience and consistency.

Figure 5 shows the 11 and 12 components of the orientation and interaction tensors for selected approximations as a function of time in simple shear flow. Results from the particle-based simulations are also presented. Numerical calculations are performed with an applied shear rate of 1 s^{-1}. The new proposed approximations (iORW-CO4P3) improve considerably the match for all components. For the a_{11}, a_{12}, and b_{12} components, it is difficult to distinguish the predictions of the both approximations up to a deformation of 15. Beyond that strain, most of the rods tumble due to the interaction forces, and the old approximations

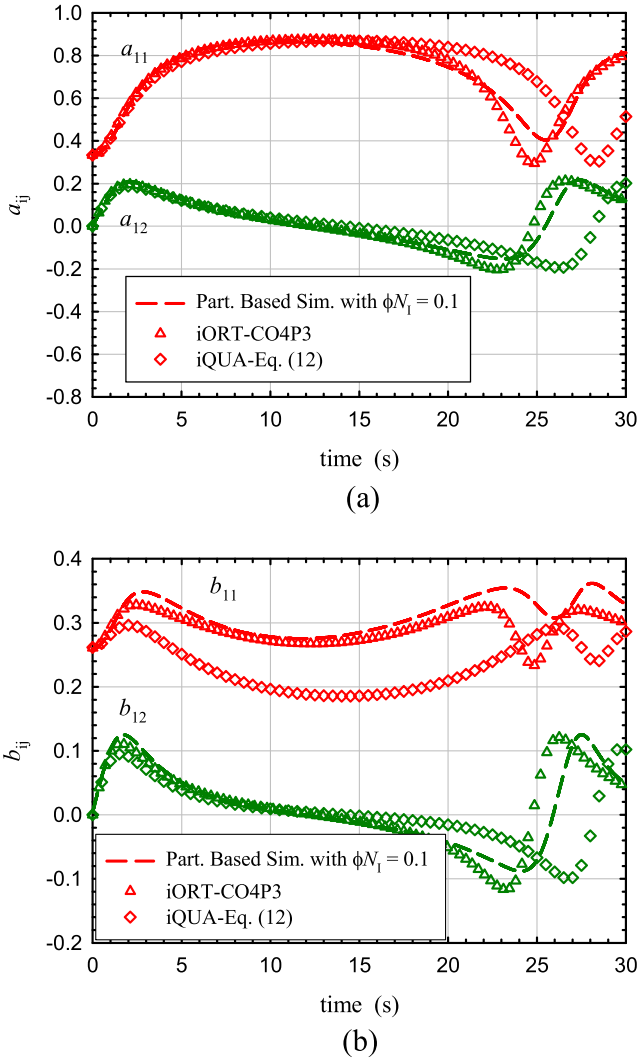

Fig. 5 Selected tensor components as functions of time in simple shear flow (shear rate $= 1\ s^{-1}$ and $\phi N_I = 0.1$). **a** Orientation tensor. **b** Interaction tensor

[iQUA-Eq. (12)] failed to predict this behavior as compared to the particle-based simulations. For the b_{11} component, its magnitude and its tumbling strain are better predicted by the new proposed approximations.

Performance in the equations of evolution

The previous tests implied homogeneous flows, that is, a steady velocity gradient is fixed at each material point. Therefore, two unsteady flows in the Lagrangian sense (i.e., combined flow test and center-gated disk flow) are used to investigate the performance for the equations of evolution of the proposed approximations (iORW-CO4P3).

Combined flow test

The combined flow test consists in three sequences of distinct homogeneous flows: a simple shear in the 1–2 direction, a shearing/stretching flow with shearing in the 2–3 direction, and stretching in 3-direction and the same shearing/stretching flow with a stronger stretching in the 1-direction. At each stage except the last one, the time required to reach the steady state is too short, so errors from one sequence carry over the initial conditions for the next period [see Cintra and Tucker (1995) for more details].

The key components of $\mathbf{a_2}$ and $\mathbf{b_2}$ are shown in Fig. 6a and b, respectively. Very faithful results are observed for the components of $\mathbf{a_2}$, as compared to the particle-based simulations where $\phi N_I = 0.1$. This suggests that the ORW3 closure approximation is well adapted to express $\mathbf{a_4}$ as ever

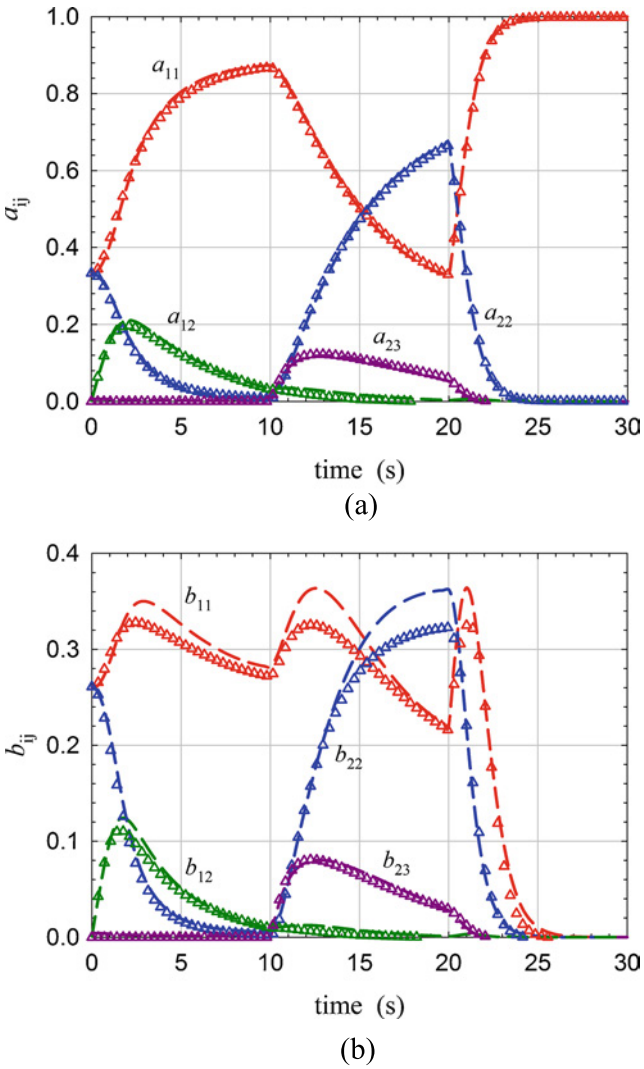

Fig. 6 Selected tensor components in combined flow test with particle-based simulations and, iORW and CO4P3 approximations. **a** Evolution of a_{11}, a_{22} and a_{12}. **b** Evolution of b_{11}, b_{22} and b_{12}

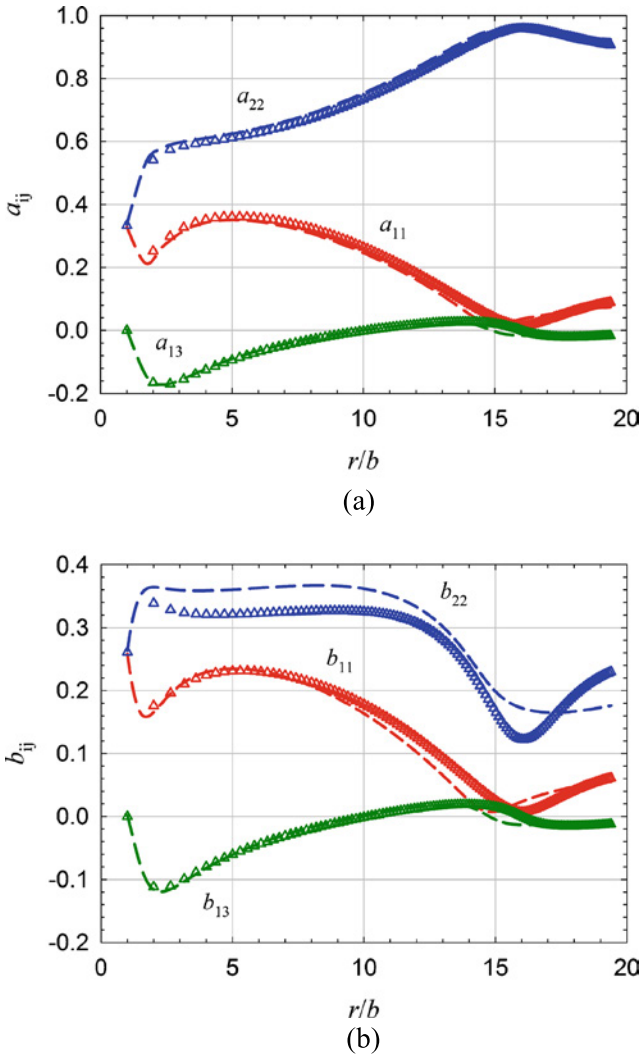

Fig. 7 Selected tensor components in isothermal Newtonian radial diverging flow using particle-based simulations and, iORW and CO4P3 approximations as a function of the radial location (r/b) at $z/b = 0.5$. **a** Evolution of a_{11}, a_{22} and a_{13}. **b** Evolution of b_{11}, b_{22} and b_{13}

used in Férec et al. (2009a), where rod-rod interactions are taken into account. For the $\mathbf{b_2}$ components, the difference between the results from the particle-based simulation and the predictions given by the proposed approximations is almost negligible. This indicates the accuracy of the couple iORW-CO4P3 for the combined flow test.

Center-gated disk flow

The second benchmark test problem is the nonhomogeneous isothermal Newtonian radial diverging flow field. This kind of flow appears in injection molding, near a pin gate or in a center-gated disk bay (Bay and Tucker 1992a, 1992b). More details dealing this flow can be found in Cintra and Tucker (1995). Altan and Rao (1995) gave an analytical solution for $\lambda_{\mathbf{p}^\alpha} = 1$ and $D_\mathrm{r} = 0$. This result will not be presented here, as we want to test the evolution of $\lambda_{\mathbf{p}^\alpha}$ with orientation [Eq. (2)].

Figure 7 reports the a_{11}, a_{22}, and a_{13} components as well as the b_{11}, b_{22}, and b_{13} at the mid gap-wise thickness position. ϕN_I is set to 0.1. For the orientation tensor components, once again, the results obtained with the proposed approximation are fairly good as compared to the one got from the particle-based simulation. Some discrepancies are observed for the interaction tensor components and especially for the 22 components. Nevertheless, the overall results are found to be satisfactory.

Our first observations show that the general framework from which the approximations are derived is of great relevance. The proposed relations seem to be quite reasonable. A natural extension of the present work can be accomplished by adding Brownian motion and testing the pseudo-shape factor, Eq. (2), for nematic polymers in order to provide some phase diagrams (Forest et al. 2004a, b, c).

Concluding remarks

We have developed a general framework to develop closure relations that is independent of the studied physic. In our case, we focused on the time evolution for rod orientation by taking into account the effect of rod-rod interactions into the hydrodynamic contributions. The obtained fittings are in agreement, indicating that our strategy is effective. Improvement of the physic such as adding rotational diffusion will change the closure coefficients.

The consideration of interactions enriches considerably the micromechanical model. By investigating only the convective part, particle-based simulations reveal that the dynamics of concentrated rod suspensions are completely modified as compared to solutions in the dilute case. It is observed that rod-rod interactions slow the orientation kinematics in systems to be more and more concentrated.

The drawback consequence of this finer description of the physic is the introduction of new conformation tensors such as interaction tensors when averaged. We derived a new closure relation to approximate the fourth-order interaction tensor, $\mathbf{b_4}$, in terms of the second-order interaction tensor, $\mathbf{b_2}$, to improve the simple linear or quadratic closures initially proposed by Férec et al. (2009a). An orthotropic fitted closure, called iORW, is developed by assuming that the principal fourth-order interaction tensor in terms of the complete second-order polynomial expansion of the three eigenvalues of $\mathbf{b_2}$.

We also justify and explain how to express $\mathbf{b_2}$ as a function of the orientation tensors. Two invariant-based optimal fitting approximations are proposed: a quadratic form is suggested, and the CO4P2 and CO4P3 expressions are

linear combinations of the second- and fourth-order orientation tensors. The coefficients that appear in the different expressions are represented by polynomial expansions in terms of the second and third invariants of the second-order orientation tensor.

For all these approximations, the unknown parameters were obtained using a least-square fitting technique with solutions calculated from the probability distribution function (PDF). Up to now, no numerical solutions exist for the Fokker-Planck equation associated with the enrich micromechanical including rod interaction due to the nonlinearity of the problem. Therefore, the generation of PDF results from a combination of the steady state solutions for simple flows without any interactions.

Numerical investigations were conducted to compare the performance between the approximations for several homogeneous flows, an unsteady combined flow, and a nonhomogeneous radial diverging flow field. The new proposed approximations exhibit more accurate results than any previous closure formula.

This work provides a way to overcome the drawback induced by the fine physic description of rod interactions. By taking into account rod-rod interaction into their micromechanical model, Férec et al. (2009a) enrich considerably the physic but introduce inevitably the use of new approximations to correctly close the overall problem. It means that micromechanical models with fine physical descriptions lead to the development of expressions, whose impacts on the final properties are not well controlled. A plausible way to overcome these problems is to solve the kinetic theories associated with the enriched micromechanical models. Classical approaches such as finite element and finite volume methods will probably failed as problems become rapidly multidimensional. We are convinced that strategies using a proper generalized decomposition will be some efficient methods.

Appendix 1

The new coefficients of iORW are as follows:

$$\overline{B}_{mm}^{\text{closure}} = C_m^1 + C_m^2\lambda_1^i + C_m^3\lambda_2^i + C_m^4\lambda_3^i + C_m^5\left[\lambda_1^i\right]^2 + C_m^6\left[\lambda_2^i\right]^2 + C_m^7\left[\lambda_3^i\right]^2 + C_m^8\lambda_1^i\lambda_2^i + C_m^9\lambda_1^i\lambda_3^i + C_m^{10}\lambda_2^i\lambda_3^i. \tag{21}$$

C_m^k	$m=1$	$m=2$	$m=3$
$k=1$	−0.002660915999438	0.003489409782309	0.001067720012882
$k=2$	0.828160371150516	0.215367759630567	0.048668855705049
$k=3$	0.789103391328429	1.720041147873011	0.094902496780697
$k=4$	0.476263752772622	0.297783383252226	0.794703264366077
$k=5$	−0.195572713563874	0.110093207391172	0.156823591195991
$k=6$	−0.968072656366994	−0.519365195025538	0.063867202721066
$k=7$	−1.288287460754669	−1.272700626531701	0.137879920843924
$k=8$	−1.227595767448560	−1.651567675520392	−0.390686023987534
v $k=9$	−0.182778698782334	0.457588594903240	−0.363326051732185
$k=10$	−1.817538271393050	−1.857949606062105	−0.510221530451348

Appendix 2

The three parameters for the CO4P2 are (note that the a_m^k coefficients are multiplied by 10^3):

$$\beta_m = a_m^1 + a_m^2 I_2 + a_m^3 I_3 + a_m^4 I_2^2 + a_m^5 I_3^2 + a_m^6 I_2 I_3. \tag{22}$$

$10^3 \cdot a_m^k$	$m=1$	$m=2$	$m=3$	$m=4$
$k=1$	−0.003218270630812	−0.062617801293020	0.119688646136867	−0.089748474872973
$k=2$	0.025608298944081	0.548145018484273	−0.917735368583849	0.667031916453076
$k=3$	−0.023906752298510	−0.489915356264443	0.822449243520880	−0.591188123665222
$k=4$	−0.047852286263352	−1.026974365711470	1.727560445560878	−1.305482024414743
$k=5$	−0.034902416392141	−0.724776286275129	1.224999080683643	−0.911112016185228
$k=6$	0.084238140388237	1.754691642707640	−2.960755852489827	2.215705673061144

Appendix 3

The three parameters for the CO4P3 are (note that the a_m^k coefficients are multiplied by 10^4):

$$\beta_m = a_m^1 + a_m^2 I_2 + a_m^3 I_3 + a_m^4 I_2^2 + a_m^5 I_3^2 + a_m^6 I_2 I_3 \quad (23)$$
$$+ a_m^7 I_2^3 + a_m^8 I_3^3 + a_m^9 I_2^2 I_3 + a_m^{10} I_2 I_3^2.$$

$10^4 \cdot a_m^k$	$m = 1$	$m = 2$	$m = 3$	$m = 4$
$k = 1$	−0.000202907175609	0.003793345630827	0.004676771640489	−0.013571219282275
$k = 2$	0.002376331912433	−0.045390224402885	−0.048495402242353	0.151520029088529
$k = 3$	−0.001962719646240	0.036071205347976	0.037591157670176	−0.117618222841952
$k = 4$	−0.009187354658680	0.185049907603453	0.163829451119346	−0.563395469982333
$k = 5$	−0.006306363944156	0.116135110250840	0.098504316934258	−0.341708656333362
$k = 6$	0.015158202494512	−0.295581503744650	−0.250908066378273	0.875038982777287
$k = 7$	0.011691632139292	−0.251081509419383	−0.177122895587727	0.691458814785002
$k = 8$	−0.006449932454001	0.125537769780743	0.077023969296916	−0.322633408773305
$k = 9$	−0.028765934401621	0.603646258346171	0.398088400923080	−1.606727456320022
$k = 10$	0.023648785610246	−0.478169447153522	−0.303053148392687	1.247489653670536

References

Abisset-Chavanne E, Mezher R, Le Corre S, Ammar A, Chinesta F (2013) Kinetic theory microstructure modeling in concentrated suspensions. Entropy 15(7):2805–2832. doi:10.3390/e15072805

Advani SG, Tucker CL (1987) The use of tensors to describe and predict fiber orientation in short fiber composites. J Rheol 31(8):751–784. doi:10.1122/1.549945

Advani SG, Tucker CL (1990) Closure approximations for three-dimensional structure tensors. J Rheol 34(3):367–386. doi:10.1122/1.550133

Altan MC, Rao BN (1995) Closed-form solution for the orientation field in a center-gated disk. J Rheol 39(3):581–599. doi:10.1122/1.550714

Ammar A, Mokdad B, Chinesta F, Keunings R (2006) A new family of solvers for some classes of multidimensional partial differential equations encountered in kinetic theory modeling of complex fluids. J Non-Newton Fluid Mech 139(3):153–176. doi:10.1016/j.jnnfm.2006.07.007

Ammar A, Mokdad B, Chinesta F, Keunings R (2007) A new family of solvers for some classes of multidimensional partial differential equations encountered in kinetic theory modelling of complex fluids: part II: transient simulation using space-time separated representations. J Non-Newton Fluid Mech 144(2-3):98–121. doi:10.1016/j.jnnfm.2007.03.009

Ausias G, Fan XJ, Tanner RI (2006) Direct simulation for concentrated fibre suspensions in transient and steady state shear flows. J Non-Newton Fluid Mech 135(1):46–57. doi:10.1016/j.jnnfm.2005.12.009

Bay RS, Tucker CL (1992a) Fiber orientation in simple injection moldings. Part I: theory and numerical methods. Polym Compos 13(4):317–331. doi:10.1002/pc.750130409

Bay RS, Tucker CL (1992b) Fiber orientation in simple injection moldings. Part II: experimental results. Polym Compos 13(4):332–341. doi:10.1002/pc.750130410

Bird RB, Curtiss CF, Armstrong RC, Hassager O (1987) Dynamics of polymeric liquids. Vol. 2, Kinetic theory, 2nd edn. Wiley, New York

Brenner H (1974) Rheology of a dilute suspension of axisymmetric Brownian particles. Int J Multiph Flow 1(4):195–341. doi:10.1016/0301-9322(74)90018-4

Bretherton FP (1962) The motion of rigid particles in a shear flow at low Reynolds number. J Fluid Mech 14(02):284–304. doi:10.1017/S002211206200124X

Chiba K, Ammar A, Chinesta F (2005) On the fiber orientation in steady recirculating flows involving short fibers suspensions. Rheol Acta 44(4):406–417. doi:10.1007/s00397-004-0422-3

Chiba K, Chinesta F (2005) Numerical simulation of flow kinematics and fiber orientation for multi-disperse suspension. Rheol Acta 45(1):1–13. doi:10.1007/s00397-004-0431-2

Chinesta F (2013) From single-scale to two-scales kinetic theory descriptions of rods suspensions. Arch Comput Method E 20(1):1–29. doi:10.1007/s11831-013-9079-3

Chinesta F, Chaidron G, Poitou A (2003) On the solution of Fokker-Planck equations in steady recirculating flows involving short fiber suspensions. J Non-Newton Fluid Mech 113(2–3):97–125. doi:10.1016/S0377-0257(03)00100-9

Chung DH, Kwon TH (2001) Improved model of orthotropic closure approximation for flow induced fiber orientation. Polym Compos 22(5):636–649. doi:10.1002/pc.10566

Cintra JS, Tucker CL (1995) Orthotropic closure approximations for flow-induced fiber orientation. J Rheol 39(6):1095–1122. doi:10.1122/1.550630

Dinh SM, Armstrong RC (1984) A rheological equation of state for semiconcentrated fiber suspensions. J Rheol 28(3):207–227. doi:10.1122/1.549748

Doi M, Edwards SF (1978) Dynamics of rod-like macromolecules in concentrated solution. Part 1. J Chem Soc Faraday T 2(74):560–570. doi:10.1039/F29787400560

Doi M, Edwards SF (1986) The rheology of polymer dynamics. Oxford Science Publications

Ericksen JL (1960) Transversely isotropic fluids. Kolloid Z 173(2):117–122. doi:10.1007/BF01502416

Fan XJ, Phan-Thien N, Zheng R (1998) A direct simulation of fibre suspensions. J Non-Newton Fluid Mech 74(1-3):113–135. doi:10.1016/S0377-0257(97)00050-5

Férec J, Ausias G, Heuzey M-C, Carreau PJ (2009a) Modeling fiber interactions in semi concentrated fiber suspensions. J Rheol 53(1):49–72. doi:10.1122/1.3000732

Férec J, Heniche M, Heuzey MC, Ausias G, Carreau PJ (2008) Numerical solution of the Fokker–Planck equation for fiber suspensions: application to the Folgar–Tucker–Lipscomb model. J Non-Newton Fluid Mech 155(1–2):20–29. doi:10.1016/j.jnnfm.2008.04.004

Férec J, Heuzey M-C, Perez-Gonzalez J, Vargas L, Ausias G, Carreau P (2009b) Investigation of the rheological properties of short glass fiber-filled polypropylene in extensional flow. Rheol Acta 48(1):59–72. doi:10.1007/s00397-008-0309-9

Folgar FP, Tucker CL (1984) Orientation behavior of fibers in concentrated suspensions. J Reinf Plast Comp 3:98. doi:10.1177/073168448400300201

Forest MG, Wang Q, Zhou R (2004a) The weak shear kinetic phase diagram for nematic polymers. Rheol Acta 43(1):17–37. doi:10.1007/s00397-003-0317-8

Forest MG, Wang Q, Zhou R (2004b) The flow-phase diagram of Doi-Hess theory for sheared nematic polymers II: finite shear rates. Rheol Acta 44(1):80–93. doi:10.1007/s00397-004-0380-9

Forest MG, Zhou R, Wang Q (2004c) Scaling behavior of kinetic orientational distributions for dilute nematic polymers in weak shear. J Non-Newton Fluid Mech 116(23):183–204. doi:10.1016/j.jnnfm.2003.07.002

Jack DA (2006) Advanced analysis of short-fiber polymer composite material behavior. University of Missouri-Columbia, PhD Dissertation

Jack DA, Schache B, Smith DE (2010) Neural network-based closure for modeling short-fiber suspensions. Polym Compos 31(7):1125–1141. doi:10.1002/pc.20912

Jeffery GB (1922) The motion of ellipsoidal particles immersed in a viscous fluid. P R Soc London 102:161–179. doi:10.1098/rspa.1922.0078

Keunings R (2004) Micro-macro methods for the multiscale simulation of viscoelastic flow using molecular models of kinetic theory. In: Binding DM, Walters KE (eds) British Society of Rheology. Rheology Reviews 2004, pp 67–98

Koch DL (1995) A model for orientational diffusion in fiber suspensions. Phys Fluids 7(8):2086–2088. doi:10.1063/1.868455

Kröger M, Ammar A, Chinesta F (2008) Consistent closure schemes for statistical models of anisotropic fluids. J Non-Newton Fluid Mech 149(1–3):40–55. doi:10.1016/j.jnnfm.2007.05.007

Larson RG (1988) Constitutive equations for polymer melts and solutions. Butterworths, Boston

Lozinski A, Owens RG, Phillips TN (2011) The Langevin and Fokker-Planck equations in polymer rheology. In: Glowinski R, Xu J (eds) Handbook of numerical analysis, vol 16, pp. 211–303. Elsevier. doi:10.1016/B978-0-444-53047-9.00002-2

Ma AWK, Chinesta F, Ammar A, Mackley MR (2008) Rheological modeling of carbon nanotube aggregate suspensions. J Rheol 52(6):1311–1330. doi:10.1122/1.2982932

Ma AWK, Chinesta F, Mackley MR (2009) The rheology and modeling of chemically treated carbon nanotubes suspensions. J Rheol 53(3):547–573. doi:10.1122/1.3093105

Morrison FA (2001) Understanding rheology. Oxford University Press, New York

Mueller S, Llewellin EW, Mader HM (2011) The effect of particle shape on suspension viscosity and implications for magmatic flows. Geophys Res Lett 38(13):L13316. doi:10.1029/2011GL047167

Onsager L (1949) The effects of shape on the interaction of colloidal particles. Ann NY Acad Sci 51:627–659. doi:10.1111/j.1749-6632.1949.tb27296.x

Petrie CJS (1999) The rheology of fibre suspensions. J Non-Newton Fluid Mech 87(2-3):369–402. doi:10.1016/S0377-0257(99)00069-5

Phelps JH, Tucker CL (2009) An anisotropic rotary diffusion model for fiber orientation in short- and long-fiber thermoplastics. J Non-Newton Fluid Mech 156(3):165–176. doi:10.1016/j.jnnfm.2008.08.002

Pruliere E, Ammar A, El Kissi N, Chinesta F (2009) Recirculating flows involving short fiber suspensions: numerical difficulties and efficient advanced micro-macro solvers. Arch Comput Method E 16(1):1–30. doi:10.1007/s11831-008-9027-9

Ranganathan S, Advani SG (1991) Fiber-fiber interactions in homogeneous flows of nondilute suspensions. J Rheol 35(8):1499–1522. doi:10.1122/1.550244

Sepehr M, Ausias G, Carreau PJ (2004) Rheological properties of short fiber filled polypropylene in transient shear flow. J Non-Newton Fluid Mech 123(1):19–32. doi:10.1016/j.jnnfm.2004.06.005

Toll S (1993) Note: on the tube model for fiber suspensions. J Rheol 37(1):123–125. doi:10.1122/1.550460

Toll S (1998) Packing mechanics of fiber reinforcements. Polym Eng Sci 38(8):1337–1350. doi:10.1002/pen.10304

Wang J, O'Gara JF, Tucker CL (2008) An objective model for slow orientation kinetics in concentrated fiber suspensions: theory and rheological evidence. J Rheol 52(5):1179–1200. doi:10.1122/1.2946437

Yamamoto S, Matsuoka T (1996) Dynamic simulation of microstructure and rheology of fiber suspensions. Polym Eng Sci 36(19):2396–2403. doi:10.1002/pen.10638

Yamanoi M, Maia JM (2010a) Analysis of rheological properties of fibre suspensions in a Newtonian fluid by direct fibre simulation. Part 1: rigid fibre suspensions. J Non-Newton Fluid Mech 165(19–20):1055–1063. doi:10.1016/j.jnnfm.2010.05.003

Yamanoi M, Maia JM (2010b) Analysis of rheological properties of fiber suspensions in a Newtonian fluid by direct fiber simulation. Part 3: behavior in uniaxial extensional flows. J Non-Newton Fluid Mech 165(23-24):1682–1687. doi:10.1016/j.jnnfm.2010.09.006

Yamanoi M, Maia JM (2011) Stokesian dynamics simulation of the role of hydrodynamic interactions on the behavior of a single particle suspending in a Newtonian fluid. Part 1. 1D flexible and rigid fibers. J Non-Newton Fluid Mech 166(9–10):457–468. doi:10.1016/j.jnnfm.2011.02.001